Applied Catalysis A: General 358 (2009) 73–78

Contents lists available at ScienceDirect

Applied Catalysis A: General

journal homepage: www.elsevier.com/locate/apcata

Mesoporous titania directly modified with tungstophosphoric acid: Synthesis, characterization and catalytic evaluation

Vanesa Fuchs, Leticia Méndez, Mirta Blanco, Luis Pizzio *

Centro de Investigación y Desarrollo en Ciencias Aplicadas "Dr. J. J. Ronco" (CINDECA), Departamento de Química, Facultad de Ciencias Exactas, UNLP-CCT La Plata, CONICET, 47 No. 257, 1900 La Plata, Buenos Aires, Argentina

ARTICLE INFO

Article history:
Received 24 October 2008
Received in revised form 28 January 2009
Accepted 30 January 2009
Available online 6 February 2009

Keywords:
Mesoporous titania
Tungstophosphoric acid
Urea
Photocatalyst

ABSTRACT

The materials were synthesized by the sol–gel method, using titanium isopropoxide as precursor and urea as pore-forming agent. During the gelation, an alcoholic solution of tungstophosphoric acid (TPA) was added. Its concentration was varied in order to obtain TPA contents of 0, 10, 20 and 30% (w/w) in the solid. The urea was extracted with water and the solids were thermally treated between 100 and 600 °C. Mesoporous solids were obtained, with a mean pore diameter (D_p) larger than 3.1 nm. The specific surface area (S_{BET}) decreased and D_p slightly increased when the TPA content was raised. S_{BET} also diminished when the calcination temperature was increased, the decrease being lower for higher TPA contents. The X-ray diffraction patterns of the solids modified with TPA only presented the characteristic peaks of the anatase phase. The crystalline degree and the crystal size increased for higher calcination temperatures. According to the Fourier transform infrared and ^{31}P magic angle spinning-nuclear magnetic resonance spectra, the $[PW_{12}O_{40}]^{3-}$ species is the one mainly present in the solids. The *band gap* values obtained from the UV–vis diffuse reflectance spectra are slightly lower than those reported for the anatase phase. The catalytic activity of the materials in the photodegradation of methyl orange was higher when the TPA content and the calcination temperature of the samples were raised. The lower recombination degree of the photogenerated electrons and holes caused by the increase in the crystalline degree, implying a lower number of defects which act as recombination centers, and in the modified samples by TPA, due to its effect as charge trapping center, added to lower *band gap* values, are the main effects responsible for the activity increase.

1. Introduction

A large number of papers deal with TiO_2 (titania) as one of the most appropriate semiconductor materials to be employed as a photocatalyst, due to its high activity in the photodegradation of organic compounds, low cost, low toxicity, and chemical stability [1–8].

Different synthetic routes have been used to obtain TiO_2, among which those that employ the sol–gel method can be mentioned [9,10]. Mesoporous titania was first prepared by a sol–gel process and modified using a phosphated surfactant [3]. Afterward, different types of ionic and neutral surfactants were employed. More recently, low cost organic compounds have begun to be used as pore-forming agents, such as urea [11], to obtain mesoporous titania with high specific surface area.

The photocatalytic activity of titania is influenced by the crystalline structure, the specific surface area, the porosity, the particle size and the size distribution, the *band gap* (E_g), and the surface density of hydroxyl groups, among other factors [12–14]. It is generally accepted that the anatase phase is the most active of the three polymorphs of titania as a photocatalyst, while the rutile phase, which is the thermodynamically stable polymorph, although active, is a poor photocatalyst [15]. The low specific surface area and the fast recombination of the photoinduced electrons and holes are considered as being mainly responsible for the low photocatalytic activity displayed by TiO_2 in practical applications.

Several researchers have tried to obtain an increase of the TiO_2 activity and a decrease of the *band gap* energy to the visible light range. Transition metals or metal oxides were proved to be electron trappers, thus avoiding the recombination of the electron–hole pairs of TiO_2-based catalysts [16–20] and improving the photocatalytic activity. In addition, it has been reported that the light absorption is extended to the visible region when large *band gap* semiconductors are doped with suitable transition metal ions [21].

Among other attempts, different heteropolyacids have been used to modify TiO_2, in order to reduce the charge recombination.

* Corresponding author. Tel.: +54 221 421 1353; fax: +54 221 425 4477.
E-mail address: lrpizzio@quimica.unlp.edu.ar (L. Pizzio).

0926-860X/$ – see front matter © 2009 Elsevier B.V. All rights reserved.
doi:10.1016/j.apcata.2009.01.040

These compounds are widely used as oxidation as well as acid catalysts [22,23], but they were also found to be effective homogeneous photocatalysts in the oxidation of organic compounds [24], and in the degradation of organic pollutants in water [25]. The heteropolycompounds have been added to suspensions of TiO_2 [26], anchored by chemical interactions to its surface [27] or used as direct modifiers of TiO_2 prepared via sol–gel [28]. The addition of HPA to the titania matrix can also improve the density of the materials, thus making the separation of the catalyst from the reaction medium easier for its later reuse.

A novel synthesis of mesoporous titania, obtained by reactions of sol–gel type using urea as pore-forming agent, directly modified with different concentrations of a Keggin heteropolyacid, tungstophosphoric acid (TPA), is described here. The samples were thermally treated between 100 and 600 °C and thoroughly characterized by different physicochemical techniques. The aim of the present work is to correlate the catalytic activity in the methyl orange photodegradation with the properties of the solids, and to discuss the effect of the preparation variables on the dye degradation.

2. Experimental

2.1. Synthesis of TPA-modified mesoporous titania

A titanium isopropoxide (Aldrich, 26.7 g) solution was prepared in absolute ethanol (Merck, 186.6 g) under N_2 atmosphere and at room temperature, continuously stirring for 10 min. Then, 0.33 cm^3 of a 0.28 M HCl aqueous solution was slowly added in order to catalyze the sol–gel reaction. After 3 h, 120 g of a urea–ethanol–water (1:5:1 w/w) solution was added, together with an ethanol solution of tungstophosphoric acid ($H_3PW_{12}O_{40}{\cdot}23H_2O$, Fluka p.a.) under vigorous stirring. The amount of TPA was varied with the purpose of obtaining a TPA concentration of 0, 10, 20 and 30% by weight in the final solid (named TiTPA00, TiTPA10, TiTPA20, and TiTPA30, respectively). The gels were dried at room temperature, and the solids were ground into powder and extracted with distilled water for three periods of 24 h, in order to remove the urea. Finally, the solids were thermally treated at 100, 200, 300, 400, 500, and 600 °C for 2 h ($TiTPAXX_{T100}$, $TiTPAXX_{T200}$, $TiTPAXX_{T300}$, $TiTPAXX_{T400}$, $TiTPAXX_{T500}$, and $TiTPAXX_{T600}$, respectively, where XX is the TPA concentration).

2.2. Sample characterization

2.2.1. Textural properties

The specific surface area and the mean pore diameter of the solids were determined from the N_2 adsorption–desorption isotherms at the liquid-nitrogen temperature, obtained using Micromeritics ASAP 2020 equipment. The solids were previously degassed at 100 °C for 2 h.

2.2.2. Nuclear magnetic resonance spectroscopy

The ^{31}P magic angle spinning-nuclear magnetic resonance (^{31}P MAS-NMR) spectra were recorded with Bruker Avance II equipment, using the CP/MAS ^{1}H–^{31}P technique. A sample holder of 4 mm diameter and 10 mm in height was employed, using 5 μs pulses, a repetition time of 4 s, and working at a frequency of 121.496 MHz for ^{31}P at room temperature. The spin rate was 8 kHz and several hundred pulse responses were collected. Phosphoric acid 85% was employed as external reference.

2.2.3. Fourier transform infrared spectroscopy

The Fourier transform infrared (FT-IR) spectra of the solids were obtained using a Bruker IFS 66 FT-IR spectrometer and pellets in KBr in the 400–4000 cm^{-1} wavenumber range.

2.2.4. X-ray diffraction

The X-ray diffraction (XRD) patterns were recorded with Philips PW-1732 equipment with a built-in recorder, using Cu Kα radiation, nickel filter, 20 mA and 40 kV in the high voltage source, and scanning angle between 5° and 60° 2θ at a scanning rate of 1°/min.

2.2.5. Diffuse reflectance spectroscopy

The diffuse reflectance spectra (DRS) of the materials were recorded using a UV-visible Lambda 35, PerkinElmer spectrophotometer, to which a diffuse reflectance chamber Labsphere RSA-PE-20 with an integrating sphere of 50 mm diameter and internal Spectralon coating is attached, in the 250–600 nm wavelength range.

2.2.6. Photodegradation reaction

The catalytic activity of the materials was evaluated in the photodegradation of methyl orange dye in water, at 25 °C. The tests were carried out employing a 125 W high-pressure mercury lamp placed inside a Pyrex glass jacket, thermostatized by water circulation, and immersed in the dye solution contained in a 300 ml cylindrical Pyrex glass reactor. The catalyst is maintained in suspension by stirring, and air is continuously bubbled. Previously, the methyl orange solution (200 ml, 8×10^{-5} mol/l) containing 100 mg of catalyst is magnetically stirred in the absence of light for 30 min. The variation of the dye concentration as a function of the reaction time was determined by a UV-visible Lambda 35 PerkinElmer spectrophotometer of double beam, measuring the absorbance at 465 nm.

3. Results and discussion

The textural properties of the solids calcined at 100 °C, that is the specific surface area (S_{BET}) determined from the N_2 adsorption–desorption isotherm using the Brunauer–Emmett–Teller (BET) method, together with the mean pore diameter (D_p) obtained from the Barret–Joyner–Halenda (BJH) distribution are shown in Table 1. It was observed that the samples are mesoporous solids with D_p higher than 3.0 nm. The S_{BET} area decreased and D_p slightly increased when the TPA content was raised. According to the microporous specific surface area (S_{Micro}) values (Table 1), calculated using the *t*-plot method, more than 90% of the total specific surface area of the solids results from their mesoporous structure.

The S_{BET} decrease that took place when the TPA content was increased can be attributed to a lower cross-linking degree during the synthesis via sol–gel [29,30].

The N_2 adsorption–desorption isotherms of the samples calcined at 100 °C (Fig. 1) can be classified as type IV, characteristic of mesoporous materials. The solids modified with TPA presented type H2 hysteresis, while is almost absent in the $TiTPA00_{T100}$ sample.

The characteristics of the isotherms of the $TiTPA10_{T200}$, $TiTPA20_{T200}$, and $TiTPA30_{T200}$ samples were similar to those thermally treated at 100 °C. However, the hysteresis was notably higher for the $TiTPA00_{T200}$ sample, which can be classified as H1. The thermal treatments at higher temperatures did not generate notable changes in the main characteristics of the isotherms.

Table 1
Physicochemical and textural properties of the solids calcined at 100 °C.

Sample	S_{BET} (m^2/g)	S_{Micro} (m^2/g)	D_p (nm)	D_C (nm)	E_g (eV)
$TiTPA00_{T100}$	372	35	3.1	5.9	3.20
$TiTPA10_{T100}$	296	24	3.4	5.4	3.05
$TiTPA20_{T100}$	276	19	3.6	5.7	3.02
$TiTPA30_{T100}$	247	10	3.9	5.6	2.99

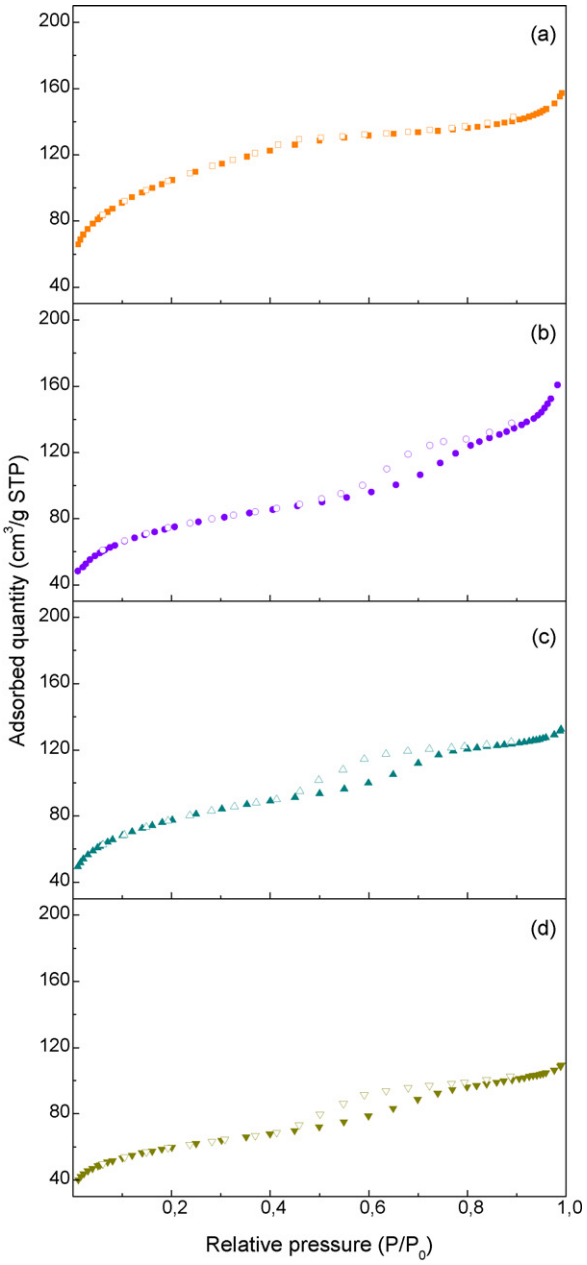

Fig. 1. N_2 adsorption–desorption isotherms of $TiTPA00_{T100}$ (a), $TiTPA10_{T100}$ (b), $TiTPA20_{T100}$ (c), and $TiTPA30_{T100}$ (d) samples.

The hysteresis of H1 and H2 types is observed in solids consisting of aggregates of spherical particles or particles crossed by cylindrical channels [31], where the pores can have uniform (H1) or nonuniform (H2) shape and size. The lower cross-linking degree during the synthesis, as a result of TPA addition, apparently leads to a less uniform or ordered mesoporous structure.

On the other hand, S_{BET} decreased when the calcination temperature was raised (Fig. 2), the microporosity of the samples disappeared and D_p slightly increased. However, the decrease in S_{BET} in the studied range (100–600 °C) is 94, 80, 75, and 62% for the TiTPA00, TiTPA10, TiTPA20 and TiTPA30 samples, respectively, showing that the decrease is lower when the TPA content is higher. This can be explained by assuming that a good distribution and interaction of the TPA added to the titania result in better separated particles, reducing their further growth, as was reported by Zhao et al. [32] for Mo, W, Cu, Fe, and Ni oxides supported on zirconia. Kumbar et al. [33] have also reported that the incorporation of TPA

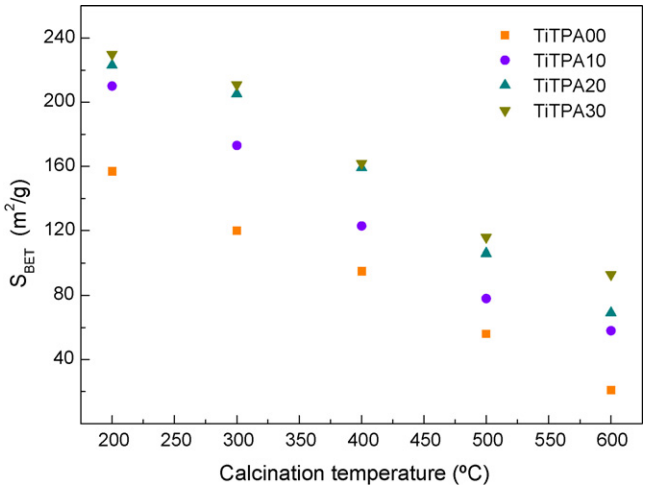

Fig. 2. S_{BET} variation as a function of temperature for the TiTPA00, TiTPA10, TiTPA20, and TiTPA30 samples.

reduces surface diffusion on titania and inhibits the sintering process. Due to these effects, it can also be observed that, unlike the behavior at 100 °C, S_{BET} of the modified samples is higher than that of the unmodified one in the range 200–600 °C (Fig. 2).

The XRD pattern of the $TiTPA00_{T100}$ sample (Fig. 3a (I)) showed weak broad peaks in the same position where the characteristic peaks of the anatase phase are placed: 25.3° (1 0 1), 37.9° (0 0 4), 47.8° (2 0 0), and 54.3° 2θ. This is indicative of a solid poorly crystallized and mostly amorphous. This effect is more marked in the samples modified with TPA calcined at 100 °C (Fig. 3b–d (I)). The intensity of the peaks became stronger with the calcination temperature rise, mainly better seen for the peaks at 25.3° 2θ. It can be well observed from the comparison of the XRD patterns of each sample at the different studied temperatures (Fig. 3a–d), and is a result of the transformation from almost amorphous to anatase phase. So, the crystalline degree of the samples increased, though to a lesser extent for the samples with higher TPA content.

The XRD pattern of the $TiTPA00_{T600}$ sample also presented peaks at 27.4° (1 1 0), 36.1° (1 0 1), and 54.2° (2 1 1) 2θ as a result of the partial phase transformation of anatase into rutile. The patterns of the TiTPA10, TiTPA20 and TiTPA30 samples only showed the characteristic peaks of the anatase phase; no diffraction line corresponding to TPA or derived species is observed indicating that the species present are highly dispersed as a non-crystalline form or as crystallites low enough to be detected by this technique. The presence of TPA delays the crystallization of anatase phase and its transformation into the rutile phase. This effect may be induced by a good TPA dispersion, similarly to results found with other oxides and doping agents, such as molybdenum or copper oxide on zirconia [32], and also for zirconia doped with nickel or aluminum [34].

The crystal size (D_C), obtained from the Scherrer equation, of the samples modified with TPA calcined at 100 °C was slightly lower than that of the unmodified titania, and it was almost independent of the TPA content (Table 1). However, the modification with TPA seems to reduce the D_C growth, since D_C increased to a lesser extent for higher TPA amounts when the calcination temperature was raised. This behavior is very common in mixed materials containing a crystalline phase and an amorphous one [35]. The partial decrease of the surface diffusion or sintering processes induced by well-dispersed TPA, which would act as a physical barrier to these phenomena, can be the reason for the observed behavior.

The FT-IR spectra of the samples directly modified with TPA distinctly showed three of the main characteristic bands of the

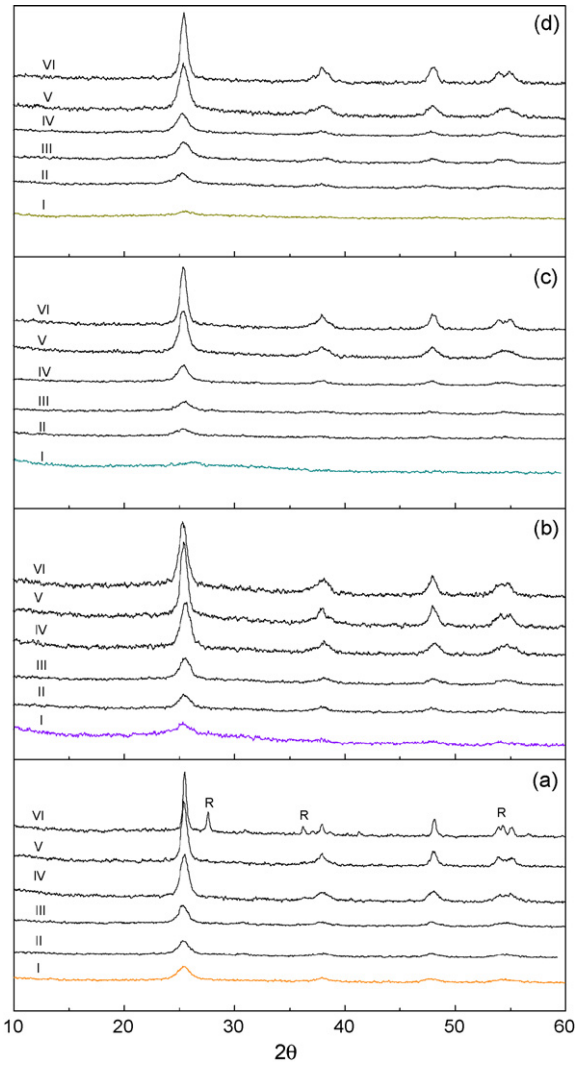

Fig. 3. XRD patterns of the TiTPA00 (a), TiTPA10 (b), TiTPA20 (c), and TiTPA30 (d) samples, calcined at 100 (I), 200 (II), 300 (III), 400 (IV), 500 (V), and 600 °C (VI).

tungstophosphate anion overlapped to the TiO_2 wide band in the 400–1200 cm^{-1} zone, and some minor bands that can be assigned to the lacunar $[PW_{11}O_{39}]^{7-}$ anion. On the other hand, two lines that can be attributed to the $[PW_{12}O_{40}]^{3-}$ anion and to the dimeric $[P_2W_{21}O_{71}]^{6-}$ species were observed by ^{31}P MAS-NMR, and also a line assigned to $[PW_{11}O_{39}]^{7-}$ anion was observed in the samples with higher TPA concentration. However, the line corresponding to the $[PW_{12}O_{40}]^{3-}$ anion is the most intense in all the samples. So, from the FT-IR and ^{31}P MAS-NMR studies, it can be established that the main species present in the titania modified with TPA is the $[PW_{12}O_{40}]^{3-}$ anion that during the synthesis and subsequent thermal treatment is partially transformed into the $[P_2W_{21}O_{71}]^{6-}$ and $[PW_{11}O_{39}]^{7-}$ species. The following transformation scheme $[PW_{12}O_{40}]^{3-} \Leftrightarrow [P_2W_{21}O_{71}]^{6-} \Leftrightarrow [PW_{11}O_{39}]^{7-}$ was proposed by Pope [36] when the pH is increased in solution. A similar change can partly take place in our samples as a result of localized pH increase during the synthesis.

The DRS of the $TiTPA00_{T100}$, $TiTPA10_{T100}$, $TiTPA20_{T100}$, and $TiTPA30_{T100}$ samples (Fig. 4) presented a continuous red-shifting of the onset of the absorption band, as a result of the titania modification with TPA. The main features of the spectra remained unchanged for the samples treated at 200 and 300 °C. However, in the spectra of the modified TiTPA10, TiTPA20, and TiTPA30 samples calcined at 400, 500, and 600 °C, a broad shoulder was

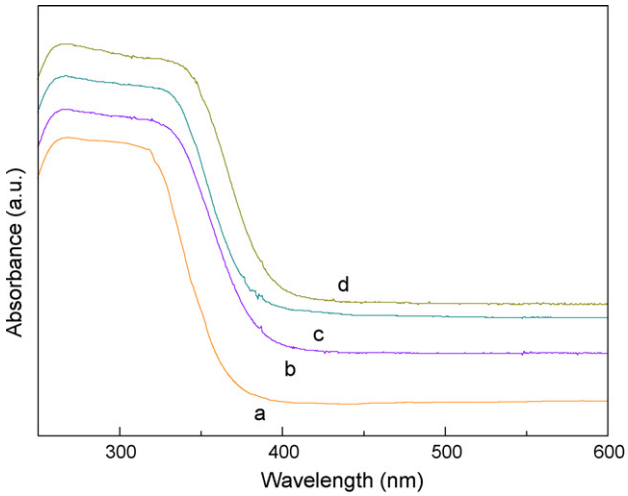

Fig. 4. DRS of the $TiTPA00_{T100}$ (a), $TiTPA10_{T100}$ (b), $TiTPA20_{T100}$ (c), and $TiTPA30_{T100}$ (d) samples.

discernible at around 450 nm, displaying the shift of the charge transfer band to wavelength values closer to that of bulk TPA. These results show the influence of tungsten species on the electronic properties of TiTPA samples.

The *band gap* values (E_g) were estimated from the corresponding Kubelka–Munk remission functions, calculated from the absorbance values of the DRS [37]. The E_g values of the modified titania slightly decreased with the TPA content (Table 1), but they remained almost constant with the temperature increase. The E_g value of the $TiTPA00_{T100}$ sample is in agreement with the one generally reported in the literature for the anatase phase [38], which is the unique phase present in the studied samples in accordance with the XRD patterns.

Azo dyes represent about one-half of the dyes actually used in the textile industry and, as a consequence, a relevant problem is related to the release of these products in the environment [39]. Removing color from wastes is often important because the presence of small amounts of dyes is clearly visible, influences the water environment considerably [40–44], and is usually required by most government regulations.

Many authors have considered that the methyl orange is the azo dye more reluctant to be degraded, and studied their photodegradation [45–49], and we have chosen it to evaluate the catalytic performance of TiTPA samples. During the photocatalytic oxidation of methyl orange, the oxidative species formed decompose the dye via a pathway from intermediates to the final carbon dioxide and some inorganic products (SO_4^{2-}, NO_3^- and NH_4^+) [39]. The formation of intermediates occurs through two primary processes: demethylation and hydroxylation [50]. The addition of a hydroxyl radical to the carbon atom linking with the azo bond is the first target for the hydroxyl radical reaction [51]. As a result of this attack, the C–N cleavage occurs [39], the chromophore group (R_1–N = N–R_2) is destroyed, and the discoloring is observed.

The photocatalytic degradation of dyes in aqueous systems can be described by a pseudo-first-order kinetics with respect to the dye concentration [52–54], which results from considering that the reaction rate follows the Langmuir–Hinshelwood model

$$r_{MO} = -\frac{dC_{MO}}{dt} = \frac{k_r K C_{MO}}{1 + K C_{MO}}$$

where r_{MO} is the degradation rate, C_{MO} is the dye concentration, and k_r and K are the reaction and adsorption constants, respectively. When C_{MO} is low, KC_{MO} is generally negligible and the reaction rate can be assumed as of pseudo-first-order with

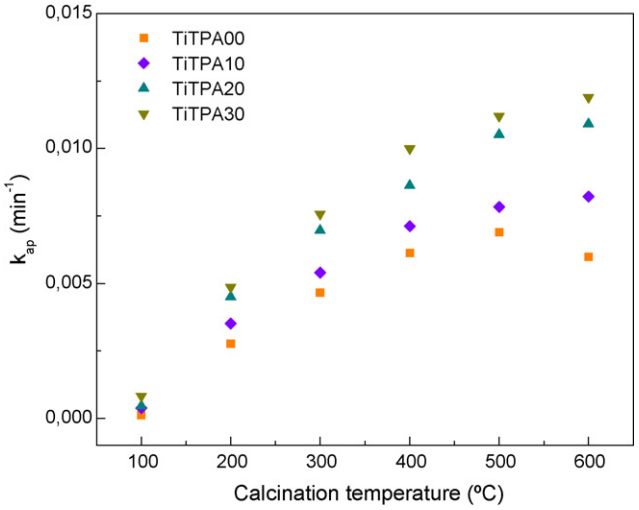

Fig. 5. Values of the apparent reaction constant k_{ap} of the TiTPA00, TiTPA10, TiTPA20 and TiTPA30 samples calcined at different temperatures.

respect to the dye concentration. The resultant equation can be integrated considering that C_{MO0} is the dye concentration at time equal zero, hence

$$\ln\left(\frac{C_{MO0}}{C}\right) = k_r K t$$

From the plots of $\ln(C_{MO0}/C)$ as a function of time, the values of the apparent reaction constant $k_{ap} = k_r K$ were obtained and are shown in Fig. 5.

The values of k_{ap} of the TiTPA00 sample in the methyl orange photodegradation increased when the calcination temperature was raised up to 500 °C, and then k_{ap} slightly diminished when the sample was calcined at 600 °C. The increase of k_{ap} is attributed to the higher crystalline degree of the sample, as was reported by Peng et al. [55] for the photocatalytic oxidation of Rhodamine B using mesoporous TiO_2 nanoparticles. As a result of such increase, the number of defects, which act as recombination centers for the photogenerated electrons and holes, diminish [15,56–59]. The appearance of the rutile phase may be responsible for the slight decrease of k_{ap} observed for the $TiTPA00_{T600}$ sample [60].

The TPA direct modification of titania led to an increment in the photocatalytic activity of titania in the reaction of methyl orange degradation. The values of k_{ap} increased with the calcination temperature and the TPA content, though the increase is lower when the TPA amount changes from 20 to 30%.

The activity in a catalytic photodegradation depends on a balance between the surface charge transfer and the recombination of electrons and holes. If the latter is decreased, there will be a higher amount of reactive species to participate in the degradation of the organic substrate. These species may be OH^*, O_2^{*-}, HO_2^*, being OH^* the more common on TiO_2 surface [15].

It has been proposed that W as doping agent in TiO_2 is easily reduced by photogenerated electrons. This reduced W species may become oxidized W by transferring electrons to oxygen or by reaction with holes. The reaction rate increase with W content may suggest that W mainly acts as a charge trapping center [61]. So, the k_{ap} increase with the TPA content in our samples may be considered indicative of the participation of TPA in the decrease of the recombination degree of photogenerated charges, as was proposed for the reaction rate of toluene photooxidation using TiO_2 doped with tungsten from ammonium tungsten oxide solutions [34]. In addition, the higher activity can also be due to the lower *band gap* values, which would increase the absorption capacity of higher wavelength radiation.

So, the use of urea as low cost pore-forming agent and the direct modification with tungstophosphoric acid of titania prepared by the sol–gel-type reaction lead to mesoporous titania with anatase polymorph as the unique titania phase present. These materials, with somewhat lower *band gap* energy, have shown a good behavior as catalysts for methyl orange photodegradation. Taking into account the results obtained in this reaction, the catalyst that gave the highest activity with the lower preparation cost is the one modified with 20% TPA calcined at 500 °C.

4. Conclusions

Mesoporous titania modified by TPA addition was synthesized by sol–gel-type reactions using urea as pore-forming agent.

The specific surface area of the samples depended on the TPA content and the subsequent thermal treatment. The titania modification with TPA reduced surface diffusion on titania or sintering process, stabilized the anatase phase, led to solids with higher S_{BET} specific surface area than the unmodified titania, and to a decrease of D_C growth. Furthermore, the TPA modification allowed obtaining lower E_g values.

The direct modification with TPA is a good method to increase the photocatalytic activity of titania in the reaction of methyl orange degradation. This study allowed us to observe the effect of the properties of the prepared catalysts, and also to choose the best preparation conditions to carry out the photocatalytic degradation. In sum, good photocatalysts with appropriate characteristics to enhance the catalytic activity through an influence on the recombination degree of the photogenerated electrons and holes were obtained.

Acknowledgements

The authors thank the experimental help of E. Soto, L. Osiglio, G. Valle, and the financial support of CONICET and UNLP.

References

[1] K.L. Yeung, S.T. Yau, A.J. Maira, J.M. Coronado, J. Soria, P.L. Yue, J. Catal. 219 (2003) 107.
[2] A. Sclafani, L. Palmisano, E. Davì, J. Photochem. Photobiol. A: Chem. 56 (1991) 113.
[3] D.M. Antonelli, Y.J. Ying, Angew. Chem. Int. Ed. Engl. 34 (1995) 2014.
[4] S. Sakthivel, M.V. Shankar, M. Palanichamy, B. Arabindoo, D.W. Bahnemann, V. Murugesan, Water Res. 38 (2004) 3001.
[5] L. Gao, Q. Zhang, Scr. Mater. 44 (2001) 1195.
[6] J.C. Yu, J. Lin, D. Lo, S.K. Lam, Langmuir 16 (2000) 7304.
[7] K.-H. Wang, H.-H. Tsai, Y.-H. Hsieh, Appl. Catal. B: Environ. 17 (1998) 313.
[8] R. Van Grieken, J. Aguado, M.J. López-Muñoz, J. Marugán, J. Photochem. Photobiol. A: Chem. 3010 (2002) 1.
[9] H. Yin, Y. Wada, T. Kitamura, S. Kambe, S. Murasawa, H. Mori, T. Sakata, S. Yanagida, J. Mater. Chem. 11 (2001) 1694.
[10] M.K. Akhtar, S. Vermury, S.E. Pratsinis, Nanostruct. Mater. 4 (1994) 537.
[11] L.R. Pizzio, Mater. Lett. 59 (2005) 994.
[12] G. Sivalingam, K. Nagaveni, M.S. Hegde, G. Madras, Appl. Catal. B: Environ. 45 (2003) 23.
[13] S.I. Nishimoto, B. Ohtani, H. Kajiwara, T. Kajiya, J. Chem. Soc., Faraday Trans. 1 (81) (1985) 61.
[14] R.I. Bickley, T. Gonzalez-Carreno, J.S. Lees, L. Palmisano, R.J.D. Tilley, J. Solid State Chem. 92 (1991) 178.
[15] J. Ovenstone, J. Mater. Sci. 36 (2001) 1325.
[16] W. Lee, Y.M. Gao, K. Dwight, A. Wold, Mater. Res. Bull. 27 (1992) 685.
[17] A. Sclafani, M.N. Mozzanega, P.J. Pichat, Photochem. Photobiol. A: Chem. 59 (1991) 181.
[18] W. Lee, Y.R. Do, K. Dwight, A. Wold, Mater. Res. Bull. 28 (1993) 1127.
[19] T. Carlson, G.L. Griffin, J. Phys. Chem. 90 (1986) 5896.
[20] S. Ikeda, N. Sugiyama, B. Pal, G. Marci, L. Palmisano, H. Noguchi, K. Uosaki, B. Ohtani, Phys. Chem. Chem. Phys. 3 (2001) 267.
[21] M. Anpo, Catal. Surv. Jpn. 1 (1997) 169.
[22] T. Okuhara, N. Mizuno, M. Misono, Adv. Catal. 41 (1996) 221.
[23] L.R. Pizzio, P.G. Vázquez, C.V. Cáceres, M.N. Blanco, Appl. Catal. A: Gen. 256 (2003) 125.
[24] E. Papaconstantinou, Chem. Soc. Rev. 18 (1989) 1.
[25] A. Mylonas, E. Papaconstantinou, J. Mol. Catal. A: Chem. 92 (1994) 261.
[26] R.R. Ozer, J.L. Ferry, Environ. Sci. Technol. 35 (2001) 3242.
[27] Y. Yang, Y. Guo, C. Hu, Y. Wang, E. Wang, Appl. Catal. A: Gen. 273 (2004) 201.

[28] V.M. Fuchs, E.L. Soto, M.N. Blanco, L.R. Pizzio, J. Colloid Interf. Sci. 327 (2008) 411.
[29] N. Phonthammachai, T. Chairassameewong, E. Gulari, A.M. Jamieson, S. Wongkasemjit, Micropor. Mesopor. Mater. 66 (2003) 261.
[30] K.M.S. Khalil, T. Baird, M.I. Zaki, A.A. El-Samahy, A.M. Awad, Colloid Surf. A 132 (1998) 31.
[31] G. Leofanti, M. Padovan, G. Tozzola, B. Venturelli, Catal. Today 41 (1998) 207.
[32] B.-Y. Zhao, X.-P. Xu, H.-R. Ma, D.-H. Sun, J.-M. Gao, Catal. Lett. 45 (1997) 237.
[33] S.M. Kumbar, G.V. Shanbhag, F. Lefebvre, S.B. Halligudi, J. Mol. Catal. A 256 (2006) 324.
[34] J.C. Duchet, M.J. Tilliette, D. Cornet, Catal. Today 10 (1991) 507.
[35] E. Ortiz-Islas, T. López, R. Gómez, M. Picquart, D.H. Aguilar, P. Quintana, Appl. Surf. Sci. 252 (2005) 853.
[36] T. Pope, Heteropoly and Isopoly Oxometalates, Springer-Verlag, Heidelberg, 1983, p. 58.
[37] S.P. Tandom, J.P. Gupta, Phys. Stat. Sol. 38 (1970) 363.
[38] E. Joselevich, I. Willner, J. Phys. Chem. 98 (1994) 7628.
[39] C. Baiocchi, M.C. Brussino, E. Pramauro, A.B. Prevot, L. Palmisano, G. Marcìl, Int. J. Mass Spectrom. 214 (247) (2002).
[40] H. Chun, W. Yizhong, Chemosphere 39 (1999) 2107.
[41] S. Ledakowicz, M. Gonera, Water Res. 33 (1999) 2511.
[42] J. Grzechulska, A.W. Morawski, Appl. Catal. B 36 (2002) 45.
[43] P. Lu, F. Wu, N.S. Deng, Appl. Catal. B 53 (2004) 87.
[44] N. Daneshvar, D. Salari, A.R. Khataee, J. Photochem. Photobiol. A 157 (2003) 111.
[45] F. Kiriakidou, D.I. Kondarides, X.E. Verykios, Catal. Today 54 (1999) 119.
[46] C. Bauer, P. Jacques, A. Kalt, J. Photochem. Photobiol. A 140 (2001) 87.
[47] J. Bandara, J.A. Mielczarski, J. Kiwi, Langmuir 15 (1999) 7670.
[48] Y. Chen, S. Yang, K. Wang, L. Lou, J. Photochem. Photobiol. A 172 (2005) 47.
[49] L. Lucarelli, V. Nadtochenko, J. Kiwi, Langmuir 16 (2000) 1102.
[50] A.B. Prevot, D. Fabbri, E. Pramauro, C. Baiocchi, C. Medana, J. Chromatogr. A 1202 (2008) 145.
[51] J.T. Spadaro, L. Isabelle, V. Renganathan, Environ. Sci. Technol. 28 (1994) 1389.
[52] K. Vinodgopal, D.E. Wynkoop, P.V. Kamat, Environ. Sci. Technol. 30 (1996) 1660.
[53] H. Lachheb, E. Puzenat, A. Houas, M. Ksibi, E. Elaloui, C. Guillard, J.-M. Herrmann, Appl. Catal. B 39 (2002) 75.
[54] K. Tanaka, K. Padermpole, T. Hisanaga, Water Res. 34 (2000) 327.
[55] T. Peng, D. Zhao, K. Dai, W. Shi, K. Hirao, J. Phys. Chem. B 109 (2005) 4947.
[56] B. Ohtani, S. Nishimoto, J. Phys. Chem. 97 (1993) 920.
[57] H. Kominami, J. Kato, S. Murakami, Y. Ishii, M. Kohno, K. Yabutani, T. Yamamoto, Y. Kera, M. Inoue, T. Inui, B. Ohtani, Catal. Today 84 (2003) 181.
[58] J.G. Yu, H.G. Yu, B. Cheng, X.J. Zhao, J.C. Yu, W.K. Ho, J. Phys. Chem. B 107 (2003) 13871.
[59] B. Ohtani, Y. Ogawa, S. Nishimoto, J. Phys. Chem. B 101 (1997) 3746.
[60] C. Su, B.-Y. Hong, C.-M. Tseng, Catal. Today 96 (2004) 119.
[61] A. Fuerte, M.D. Hernández-Alonso, A.J. Maira, A. Martínez-Arias, M. Fernández-García, J.C. Conesa, J. Soria, G. Munuera, J. Catal. 212 (2002) 1.